Please cite this article as:

Abdelkader H.S, Kheder A.A., Farroh K.Y, Shfie R.M. 2026. Nanoparticle-mediated defense and antiviral protection in roselle against *Hibiscus chlorotic ringspot virus* (HCRSV). Journal of Plant Protection Research. DOI: 10.24425/jppr.2026.2997

Original article

Nanoparticle-mediated defense and antiviral protection in roselle against *Hibiscus chlorotic ringspot virus* (HCRSV)

Hayam Samy Abdelkader[1*], Ahmed A. Kheder[1], Khaled Yehia Farroh[2], Radwa Mahmoud Shfie[1]

[1] Virus and Phytoplasma Research Department, Plant Pathology Research Institute, Agricultural Research Center, Cairo University Street, Giza, Egypt

[2] Nanotechnology and Advanced Materials Central Lab., Regional Center for Food and Feed, Agricultural Research Center, Cairo University Street, Giza, Egypt

*Corresponding address: hsabdelkader@outlook.com

Received: October 24, 2025

Accepted: January 13, 2026

Online pree-Proof Publication:

Responsible Editor: Rafał Kukawka

DOI: 10.24425/jppr.2026.2997

Abstract

Hibiscus sabdariffa (roselle) is highly susceptible to Hibiscus chlorotic ringspot virus (HCRSV), for which effective control strategies remain limited. This study assessed the antiviral and defense-priming potential of foliar-applied chitosan–silver nanocomposites (CS-Ag NCs) and copper oxide nanoparticles (CuO-NPs) at

concentrations of 50–300 ppm, applied either before or after virus inoculation. The nanomaterials were synthesized and physicochemically characterized using HR-TEM, DLS/ζ-potential, and XRD analyses. Both CS-Ag NCs and CuO-NPs significantly reduced HCRSV infection incidence in a dose-dependent manner, with the strongest curative effects observed at 300 ppm post-inoculation (CS-Ag ≈ 91.7% and CuO ≈ 85%), without visible phytotoxic effects under greenhouse conditions. CS-Ag NC treatment markedly enhanced host defense capacity, as reflected by increased activities of antioxidant and phenylpropanoid-related enzymes (PAL, POX, and CAT), elevated phenolic and anthocyanin contents, and improved sepal yield (222.6 g plant^{-1} compared to 133.2 g plant^{-1} in infected controls). Gene-expression profiling ($2^{-\Delta\Delta Ct}$) revealed strong CS-Ag-mediated induction of sulfur redox–associated genes, particularly sulfite oxidase (*SO*) and APS kinase (*APK*), indicating reinforcement of redox homeostasis and reactive oxygen species detoxification pathways. In contrast, adenylylsulfate reductase (*APR*) exhibited a biphasic, dose-dependent transcriptional response, suggesting that sulfur assimilation is finely regulated and sensitive to both nanomaterial type and stress intensity. Collectively, these findings indicate that CS-Ag NCs predominantly act as defense-priming agents that enhance sulfur-linked antioxidant signaling, whereas CuO-NPs confer antiviral protection in a more dose- and stress-dependent manner. This study provides mechanistic insight into nano-enabled antiviral defense in roselle and identifies practical dose–timing windows for disease management, while underscoring the need for field-level validation and environmental safety assessment prior to large-scale application.

Keywords: copper oxide nanoparticles, HCRSV, chitosan–silver nanocomposites, defense-related genes, antiviral nanotechnology

1. Introduction

Hibiscus sabdariffa L. (roselle), a member of the Malvaceae family, is widely known as roselle, hibiscus, or red sorrel in English and *karkadeh* in Arabic (**Ross 2003; Ali *et al.* 2005**). It is cultivated across tropical and subtropical regions, and various parts of the plant-flowers, leaves, calyces, and corollas are used in traditional medicine for treating hypertension, hyperlipidemia, liver disorders, and inflammatory conditions (**Babajide *et al.* 2004**). The dried calyces are commonly brewed into hibiscus tea, rich in phenolic compounds, anthocyanins, flavonoids, vitamins, minerals, and dietary fiber, which contribute to its antioxidant and therapeutic properties (**Fasoyiro *et al.* 2005;**

Hassan 2009; Abou-Sreea *et al*. 2022). Owing to these bioactive constituents, roselle has significant applications in the food, pharmaceutical, and cosmetic industries.

Despite its nutraceutical and economic importance, roselle is highly susceptible to viral infections, particularly *Hibiscus chlorotic ringspot virus* (HCRSV), a member of the *Tombusviridae* family that induces severe mosaic, chlorotic and ring spots, vein banding, chlorosis, leaf distortion, and leaf cupping (**Niu *et al*. 2014; Shafie 2019**). The virus is transmitted mechanically and through vegetative propagation rather than via seeds or insect vectors (**Brunt and Spence 2000**). HCRSV has been reported in several roselle-growing regions, including Egypt, where it represents a major constraint to crop productivity (**Shafie 2019**).

From an economic perspective, HCRSV infection leads to substantial yield and quality losses in roselle by reducing leaf area, impairing photosynthetic efficiency, and markedly decreasing calyx size, weight, and pigment content, which directly affects marketability and export value. Field observations and experimental studies have reported severe symptom development associated with significant reductions in biomass and calyx yield, with losses frequently described as economically damaging at the farm level (**Brunt and Spence 2000; Niu *et al*. 2014; Shafie 2019**). Although precise global loss percentages attributable solely to HCRSV have not yet been systematically quantified, localized reports indicate that viral infection can render roselle fields partially or completely unmarketable, particularly when infection occurs at early growth stages.

To date, management of HCRSV has been largely limited to preventive and cultural practices, including the use of virus-free planting material, sanitation, and avoidance of mechanical transmission. Previous research on HCRSV has focused mainly on virus detection, molecular characterization, and host–virus interactions rather than on disease control or therapeutic intervention (**Brunt and Spence 2000; Niu *et al*. 2014; Shafie 2019**).

In recent years, nanoparticles have attracted increasing attention in agrobiotechnology not only for their antimicrobial properties, but also for their capacity to enhance plant growth, physiology, and beneficial plant–microbe interactions. Several studies have demonstrated that engineered nanomaterials can stimulate photosynthesis, improve nutrient uptake, and promote rhizosphere competence without adverse environmental effects when applied at optimized doses. For example, titanium dioxide nanoparticles were reported to support the formation of functional rhizobiotic structures and

beneficial root–microbe associations, contributing to improved plant performance under stress conditions (**Przemieniecki *et al.* 2025**). Likewise, copper-based nanoparticles have been shown to enhance photosynthetic efficiency and nutrient assimilation in plants, highlighting their dual role as both protective and growth-supportive agents (**Raza *et al.* 2024**).

Chitosan, a natural biopolymer derived from chitin, is biodegradable, non-toxic, and environmentally compatible. Beyond its well-documented antimicrobial and antiviral activities, chitosan functions as a plant defense elicitor and growth-supporting agent by modulating hormonal balance, antioxidant capacity, and cell-wall reinforcement. Its cationic nature and reactive amino and hydroxyl groups enable effective interaction with plant tissues, leading to induced systemic resistance in crops such as tomato, cucumber, potato, sunflower, and tobacco (**Davydova *et al.* 2011; Hassan 2017; He *et al.* 2021**). Nanotechnological modification of chitosan further enhances these beneficial properties by increasing surface reactivity and facilitating controlled interaction with plant defense and metabolic pathways (**Chandra *et al.* 2015**).

Nanomaterials are increasingly recognized as multifunctional tools in sustainable agriculture, combining antimicrobial efficacy with growth-promoting and stress-mitigating functions when judiciously applied. Their high surface-to-volume ratio and tunable physicochemical properties allow targeted modulation of plant physiological and immune responses while minimizing chemical inputs (**Fernando *et al.* 2018; Cai *et al.* 2019; Bhandari *et al.* 2023**). Chitosan-based nanostructures, in particular, have shown strong antiviral performance against several plant viruses, including *Alfalfa mosaic virus*, *Bean yellow mosaic virus*, and *Tobacco mosaic virus*, while maintaining favorable environmental profiles (**Abdelkhalek *et al.* 2021; El Gamal *et al.* 2022; El-Ganainy *et al.* 2023**).

Similarly, copper oxide nanoparticles (CuO-NPs) exhibit antiviral activity while also participating in essential plant metabolic processes, as copper is a micronutrient involved in photosynthesis and redox regulation. When applied at appropriate concentrations, CuO-NPs have been reported to reduce disease severity and viral accumulation without inducing phytotoxicity (**Nikolova and Chavali 2020; Derbalah *et al.* 2022; Liu *et al.* 2024**).

However, despite the documented economic impact of HCRSV and the growing success of nanomaterials in plant virus management, their application against HCRSV in roselle remains unexplored. Therefore, this study represents the first attempt to

evaluate nanomaterial-mediated antiviral protection against HCRSV, comparing chitosan–silver nanocomposites and copper oxide nanoparticles for their ability to reduce disease severity and enhance host defense responses at biochemical and molecular levels.

2. Materials and Methods

2.1 Greenhouse experiment

Experiments were performed in a completely randomized design under greenhouse conditions using *Hibiscus sabdariffa* plants. Each treatment included 10 plants, and the experiment was independently repeated twice at four-week intervals under identical conditions (25 ± 2°C, 60–70% relative humidity). Treatment effects were evaluated across both experiments while statistically controlling for differences between experimental runs.

2.2 Virus Source and Propagation

The *Hibiscus chlorotic ringspot virus* (HCRSV) isolate, previously identified by **Shafie (2019)**, was purified through three single-lesion passages on *Chenopodium amaranticolor* and subsequently propagated in healthy *H. sabdariffa* cv. Aswan plants maintained under greenhouse conditions (25 ± 2°C, natural daylight, 60–70% RH). Sap from symptomatic leaves was used for mechanical inoculation, and symptom expression was monitored for three weeks.

2.3 Infection Assessment

For each treatment, infection incidence was calculated as the number of infected plants / 10 × 100. Plants were observed daily up to 21 days post-inoculation, and infection was confirmed by RT-PCR using HCRSV coat-protein–specific primers. Non-inoculated controls remained symptom-free and tested negative, confirming no cross-contamination.

2.4 Molecular Detection and Quantitative Analysis

Total RNA was extracted from 100 mg of symptomatic *Hibiscus sabdariffa* leaf tissue using the FavorGen kit (Cat. No. FATRS 100; Biotech Corp) according to the manufacturer's instructions. RNA integrity and purity were assessed spectrophotometrically and by agarose gel electrophoresis. Complementary DNA (cDNA) was synthesized using the Verso 1-Step RT-PCR Kit (Thermo Scientific, USA). The presence of *Hibiscus chlorotic ringspot virus* (HCRSV) was confirmed by PCR amplification of the coat-protein (CP) gene using specific primers **(Table 1) (Tang *et al.* 2008; Gao RuiMin *et al.* 2012).** The expected 557 bp amplicon was

visualized on a 1.5% agarose gel stained with ethidium bromide. Quantitative RT-PCR (qRT-PCR) was performed to assess the expression of defense-related genes using the Verso 1-Step RT-qPCR Kit with SYBR Green on a QuantStudio™ 5 Real-Time PCR System (Thermo Scientific). Each 5 µL reaction contained 1 µL RNA template and 0.1 µL of each primer (10 µM). Cycling conditions were: reverse transcription at 50°C for 15 min, initial denaturation at 95°C for 10 min, followed by 40 cycles of 95°C for 15 s and 60°C for 1 min, with a melt-curve stage from 60–95°C (0.3°C/s). Primer efficiencies ranged from 90 to 110%. *Actin* served as the internal reference gene, and relative expression levels were calculated using the $2^{-\Delta\Delta Ct}$ method. Non-inoculated controls were included in each run and consistently tested negative, confirming assay specificity and the absence of contamination. Melt-curve analysis confirmed the specificity of all qRT-PCR amplifications, with single, well-defined peaks and no evidence of primer–dimer formation; representative melt curves are provided in the Supplementary Materials.

Table 1. Primers Used for qRT-PCR Analysis of Defense-Related Gene Expression in *Hibiscus sabdariffa*

Gene	Primer name	Sequence (5′→3′)	References
Coat protein (CP) of HCRSV	CP-F	GGAACCCGTCCTGTTACTTC	**Tang *et al.* (2008)**
	CP-R	ATCACATCCACATCCCCTTC	
Sulfite oxidase (*SO*)	SO-qF247	ATGTCAGGATGCTGCCAAAAT	**Gao RuiMin *et al.* (2012)**
	SO-qR381	TGCTCATGGCAGTCCTCCTCTAT	
APS kinase (*APK*)	APK-qF72	GTTGGGTTACATACCTTGATGGTG	
	APK-qR206	TGAGTCCAGCACATCAGCAAAGA	
5′-Adenylylsulfate reductases (*APR*)	APR-qF239	TGAAGTGGAACCCCTGTTGCC	
	APR-qR343	TGGACACAAATCCTTGGGGAATG	
Actin	Act-qF603	ACGAGCAGGAACTGGAGACT	
	Act-qR734	TGAGTGATGGCTGGAAGAGGA	

2.5 Experimental treatments and application schedule

The antiviral activity of chitosan–silver nanocomposites (CS–Ag NCs) and copper oxide nanoparticles (CuO–NPs) against HCRSV was evaluated under greenhouse conditions using two experimental approaches: a protective treatment (pre-inoculation) and a curative treatment (post-inoculation). For the protective assay, plants were sprayed with the nanoparticle suspension 24 hours before mechanical inoculation (−24 h). For the curative assay, spraying was performed 24 hours after virus inoculation (+24 h). Each treatment consisted of 10 roselle plants (cv. Aswan) per replicate, and the experiment was repeated twice under identical environmental conditions. The nanoparticle suspensions were applied to the foliage until runoff using a hand-held atomizer equipped with a fine mist nozzle, delivering approximately 10 ml per plant. To control for handling effects, mock-treated control plants were sprayed with distilled water following the same schedule. Non-inoculated control plants were maintained separately under identical conditions to monitor for accidental infection.

2.6 Synthesis of CS-Ag NCs

Chitosan–silver nanocomposites (CS-Ag NCs) were synthesized following the method of **Babu *et al.* (2017)** with minor modifications. Briefly, a 1% (w/v) chitosan solution (50,000–190,000 Da, 75–85% deacetylation; Sigma-Aldrich) was prepared in 1% (v/v) acetic acid under constant magnetic stirring. A 0.01 M $AgNO_3$ solution was then added dropwise and stirred for 2 h at room temperature, followed by the slow addition of 20 mL of freshly prepared 0.04 M $NaBH_4$, which induced a visible color change from pale yellow to brown, indicating nanoparticle formation. The resulting suspension was centrifuged at 20,000 × g for 30 min, washed three times with deionized water to remove unreacted ions, resuspended, and finally freeze-dried to obtain the nanocomposite powder. The final yield was approximately 0.42 g of dry powder per 100 mL reaction, and the resulting CS-Ag NC suspensions were stored at 4°C in dark amber vials until use (≤ 30 days) to prevent photodegradation and aggregation.

2.7 Synthesis of CuO-NPs

CuO-NPs were synthesized via chemical precipitation following **Luna *et al.* (2015)** with modifications. A 0.5 M $CuCl_2 \cdot 2H_2O$ solution (Sigma-Aldrich, USA) was prepared in ethanol, and 100 mL of 1 M NaOH (≥99.9% purity) was added dropwise under constant stirring at room temperature. The reaction mixture gradually turned black, indicating nanoparticle formation. The precipitate was collected by centrifugation, washed repeatedly with ethanol and deionized water, dried under vacuum at 50°C, and annealed at 400°C for 4 h to enhance crystallinity. Morphological, structural, and

surface characterizations were performed as described for Ch–Ag NCs, using HR-TEM (Tecnai G2, FEI, Netherlands), DLS and zeta potential (Zetasizer Nano ZS, Malvern, UK), and XRD (X'Pert PRO, PANalytical, Netherlands).

2.8 Characterization of Synthesized Nanoparticles

Morphology of Ch–Ag NCs and CuO-NPs was examined by high-resolution TEM (Tecnai G2, FEI, Netherlands) at 200 kV after 5 min sonication and deposition on carbon-coated copper grids. A Zetasizer Nano ZS (Malvern, UK) was used to measure particle size distribution and zeta potential. Crystal structure was analyzed using X-ray diffraction (X'Pert PRO, PANalytical, Netherlands) with Cu Kα radiation (λ = 1.54 Å, 40 kV, 30 mA), and diffraction peaks were compared to ICCD standards (PDF4 software). All synthesis and analysis work was performed at the Nanotechnology and Advanced Materials Central Laboratory (NAMCL), Agricultural Research Center, Egypt.

2.9 Effect of Ch–Ag NCs and CuO-NPs on Virus Infectivity and Yield of Roselle

The efficacy of Ch–Ag NCs and CuO-NPs in reducing viral infectivity and improving yield was assessed in roselle plants (*Hibiscus sabdariffa*) under greenhouse conditions. Seeds obtained from the Faculty of Agriculture, Giza, Egypt, were sown in 40 × 40 cm plastic pots and maintained under standard agronomic practices. After three weeks, seedlings were thinned to five plants per pot. Treatments were arranged in three replicates per group.

Two treatment strategies were evaluated: (i) seedlings treated with Ch–Ag NCs and/or CuO-NPs 24 h before inoculation (protective treatment), and (ii) seedlings treated 24 h after inoculation (curative treatment). Control groups included: (a) infected untreated plants (inoculated control), (b) healthy untreated plants (healthy control), (c) healthy plants treated with Ch–Ag NCs, and (d) healthy plants treated with CuO-NPs. For inoculation, 1 mL of infectious sap was mechanically applied per plant. Plants were observed daily for symptom development.

The inhibitory effect was calculated following **Devi *et al.* (2004)** using the formula:

$$\text{Inhibition } (\%) = \frac{A - B}{A} \times 100$$

where A = Number of symptomatic plants in the infected untreated control group (i.e., plants inoculated with the virus but not treated with nanoparticles). B = Number of

symptomatic plants in the treated group (i.e., those that received Ch–Ag NCs or CuO-NPs).

Growth and yield parameters were measured at different stages. Plant height (cm) and number of branches per plant were recorded six months after planting. At harvest, the number of calyces per plant and the fresh weights of sepals were determined. Twenty days after flowering, sepals were collected from healthy, treated, and infected plants, oven-dried at 70°C for 6 h, and weighed. Dried sepals were stored in a desiccator until further analyses.

2.10 Chemical Analysis of Roselle Sepals

Biochemical traits of roselle sepals were analyzed at the National Organization for Drug Control and Research, Egypt. Total titratable acidity was determined according to **AOAC (1965)** and expressed as % citric acid equivalents. Ascorbic acid content was quantified following the method of **Loeffler and Ponting (1942)** and expressed as mg/100 g FW. Total anthocyanin concentration was measured as mg/g dry weight using the methods of **Fuleki and Francis (1968)** and **Du and Francis (1973)** at 535 nm. Total phenolic content was determined according to **Malik and Singh (1980)** and expressed as mg/100 g fresh weight, with absorbance measured at 650 nm. All biochemical assays were conducted in triplicate (n = 3) for each treatment group.

2.11 Enzyme Determination in Roselle Leaves

Leaf samples from treated roselle plants were collected 21 days after inoculation with *Hibiscus chlorotic ring spot virus* (HCRSV). For each treatment, 10 g of fresh leaf tissue was used per replicate. Enzyme extraction was carried out following **Anand *et al.* (2007)**. Leaf tissues were immediately homogenized in liquid nitrogen, and 1 g of powdered tissue was extracted with 2 mL of 0.1 M sodium phosphate buffer (pH 7.0) at 4°C.

Peroxidase (POX) activity was quantified spectrophotometrically by measuring the oxidation of pyrogallol in the presence of H_2O_2 at 470 nm (**Maxwell and Bateman 1967**). Superoxide dismutase (SOD) activity was determined according to **Giannopolitis and Ries (1977)** by monitoring the inhibition of photochemical

reduction of nitroblue tetrazolium (NBT). Polyphenol oxidase (PPO) activity was assayed following **Galeazzi *et al.* (1981)** by measuring the oxidation of catechol at 420 nm. All enzyme assays were performed in triplicate (n = 3) for each treatment group.

2.12 Controls and contamination prevention

Appropriate controls were included in all greenhouse experiments. Non-inoculated healthy plants (N = 10) were maintained as negative controls to verify the absence of spontaneous or mechanical infection. These plants showed no visible symptoms (0/10) and produced no detectable HCRSV amplicon by RT-PCR.

In addition, "healthy + nanoparticle" groups (healthy plants sprayed with CS–Ag NCs or CuO–NPs at 300 ppm) were included to evaluate any possible phytotoxic or stress effects of the nanoparticles alone. These plants also remained symptom-free (0/10) and tested negative for HCRSV infection.

To minimize cross-contamination, all inoculation and sampling procedures were conducted under insect-proof greenhouse conditions. Separate benches were used for infected and control plants. Inoculations were performed from healthy to infected treatments using freshly sterilized tools (70% ethanol and sodium hypochlorite rinse) for each plant. Personnel wore disposable gloves and disinfected surfaces between treatments to prevent mechanical virus transfer.

2.13 Statistical analysis

Incidence data (number of infected plants / total inoculated) were analyzed using a binomial generalized linear mixed model (GLMM) with a logit link function. Fixed effects included treatment (CS–Ag NCs, CuO–NPs, and control), application timing (pre- or post-inoculation), and their interaction, while experimental run was incorporated as a random intercept to account for temporal variation. The model was fitted in R software (version 4.3.2) using the *lme4* package with the following syntax:

glmer (cbind(infected, total − infected) ~ treatment × timing + (1 | run), family = binomial, data = dataset)

Pairwise comparisons among estimated marginal means were performed using Tukey's post-hoc adjustment implemented in the *emmeans* package.

Continuous response variables (biochemical parameters, enzyme activities, pigment content, and growth traits) were analyzed using linear mixed models (LMMs) with treatment and timing as fixed effects and run as a random effect. Normality and

homogeneity of residuals were verified using Shapiro–Wilk and Levene's tests, respectively. When assumptions were violated, rank-based ANOVA or suitable data transformations were applied prior to re-analysis.

Results are presented as estimated marginal means ± standard error (SE), with significant differences denoted by compact letter displays from Tukey's HSD test ($\alpha = 0.05$). All analyses were performed in R (version 4.3.2) using the *lme4* and *emmeans* packages, and results were cross-validated with StatGraphics and CoStat software to ensure consistency of outputs.

3. Results

3.1 Virus isolation and propagation

The virus employed in this study was isolated from naturally infected roselle (*Hibiscus sabdariffa* L.) plants collected from Giza Governorate, Egypt. Symptomatic leaves exhibited typical signs of *Hibiscus chlorotic ring spot virus* (HCRSV) infection, including chlorotic spots, ring spots, mosaic, vein banding, bleaching, leaf chlorosis, and cupping. Mechanical inoculation successfully transmitted the virus from infected to healthy roselle seedlings (cv. Aswan) grown under greenhouse conditions, with characteristic symptoms developing 21 days post-inoculation. For purification, the virus was biologically cloned through single local lesions on *Chenopodium amaranticolor* Coste and Reyn. The purified isolate was propagated in roselle plants, which were used as a source of virus in further assays. (**Fig. 1**).

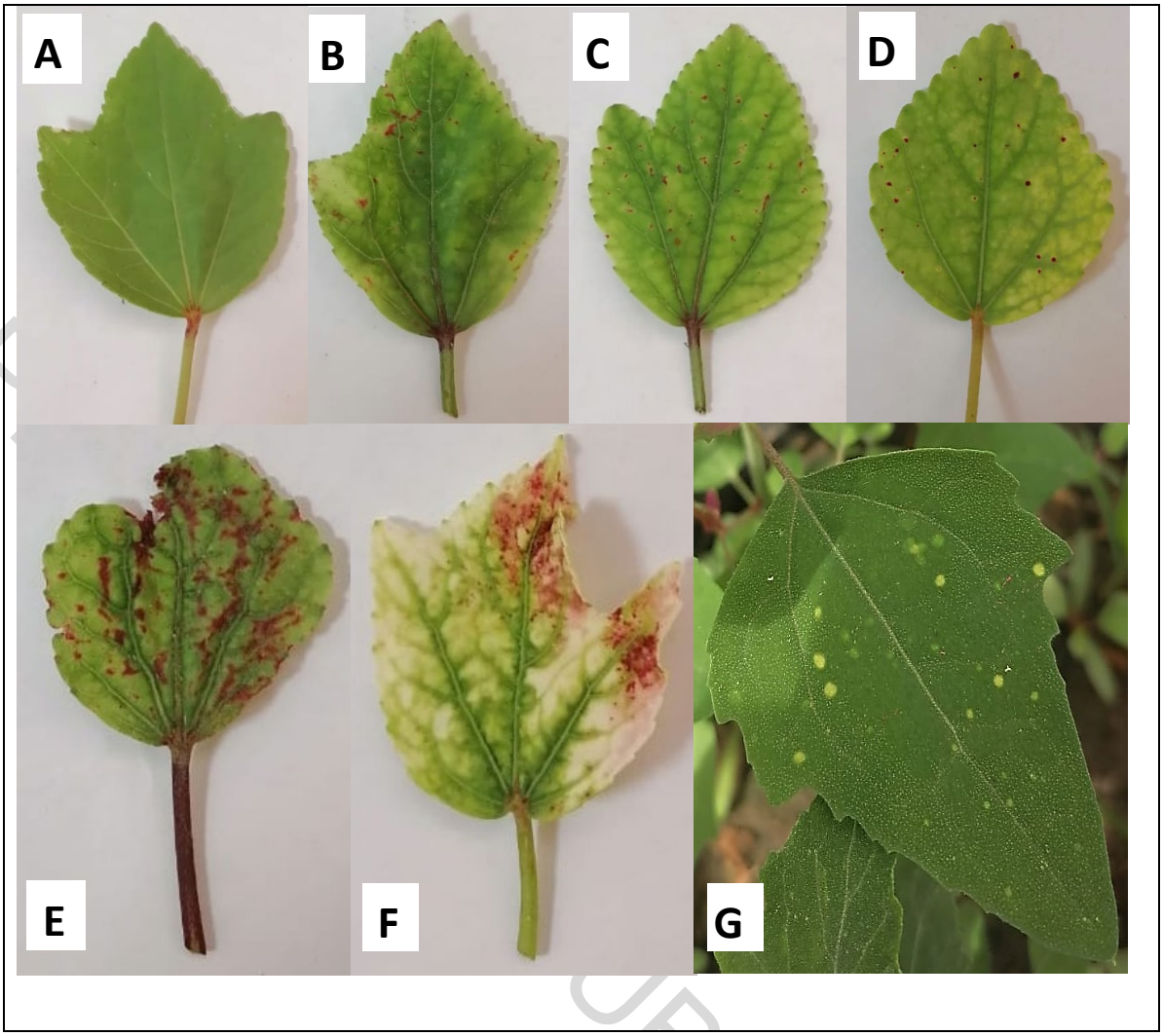

Fig.1. Symptom expression of Hibiscus chlorotic ringspot virus (HCRSV) on roselle (*Hibiscus sabdariffa* L. cv. Aswan) and the local lesion host *Chenopodium amaranticolor* under greenhouse conditions. (A) Healthy control roselle leaf. (B–E) Roselle leaves mechanically inoculated with HCRSV, showing typical symptoms including mosaic, chlorotic spots, ring spots, vein banding, bleaching, leaf chlorosis, and deformation. (F) *C. amaranticolor* leaf displaying characteristic chlorotic local lesions following inoculation with HCRSV.

3.2 Nanoparticles characterization

3.2.1 Chitosan–Silver Nanocomposites

The physicochemical properties of the synthesized chitosan–silver nanocomposites (CS-Ag NCs) were characterized using multiple analytical techniques (**Fig. 2**). High-resolution transmission electron microscopy (HR-TEM) revealed well-dispersed, spherical nanoparticles with smooth surfaces and an average diameter of ~14 nm (**Fig. 2A**), indicating efficient cross-linking between chitosan and silver.

Dynamic light scattering (DLS) analysis confirmed a hydrodynamic size of 18.2 nm, while zeta potential measurements indicated a surface charge of +65 mV (**Fig. 2B** and **2C**). The high positive zeta potential suggests excellent colloidal stability attributable to the cationic nature of chitosan.

X-ray diffraction (XRD) analysis further validated the crystalline structure of the CS-Ag NCs (**Fig. 2D**). Prominent diffraction peaks at 2θ values of 38.13°, 64.46°, and 77.42° corresponded to the (111), (220), and (311) planes, respectively. These reflections are characteristic of a face-centered cubic (fcc) structure of metallic silver and matched the standard JCPDS card no. 04-004-8730, confirming the crystalline nature of the nanocomposites.

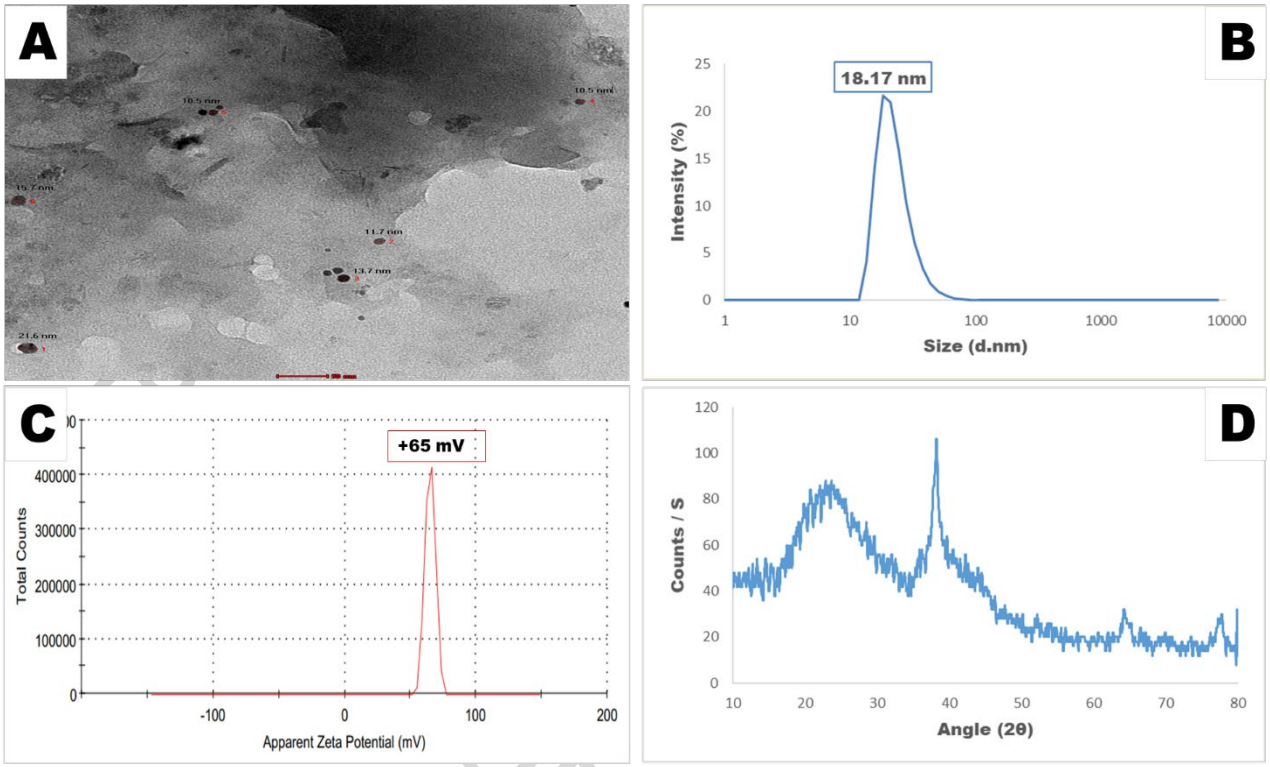

Fig 2. Characterization of chitosan–silver nanocomposites (CS-Ag NCs). (A) HR-TEM micrograph showing the morphology of the synthesized nanocomposites. (B) Zeta-potential profile indicating positive surface charge and colloidal stability. (C) Particle-size distribution histogram. (D) X-ray diffraction (XRD) pattern confirming crystalline silver–chitosan nanocomposite formation.

3.2.2 Copper Oxide Nanoparticles (CuO-NPs)

The physicochemical properties of the synthesized copper oxide nanoparticles (CuO-NPs) were characterized using HR-TEM, DLS, zeta potential, and XRD analyses (**Fig. 3**). HR-TEM imaging revealed that the CuO-NPs possessed a nearly spherical morphology with smooth surfaces and an average particle diameter of ~41.1 nm (**Fig. 3A**). Dynamic light scattering (DLS) confirmed an average hydrodynamic size of 43.8 nm, while zeta potential analysis indicated a surface charge of +35.8 mV (**Figs. 3B** and

3C). The moderately high zeta potential reflected good colloidal stability. X-ray diffraction (XRD) analysis further confirmed the crystalline structure of the CuO-NPs (**Fig. 3D**). Distinct peaks at 2θ values of 32.48°, 35.54°, 38.64°, 48.85°, 61.52°, 65.66°, 66.34°, and 68.02° corresponded to the (110), (−111), (111), (−202), (−113), (022), (−311), and (220) planes, respectively. These reflections are characteristic of the monoclinic crystalline phase of CuO and are in agreement with the standard JCPDS card no. 04-005-4712, confirming the successful synthesis of phase-pure nanoparticles.

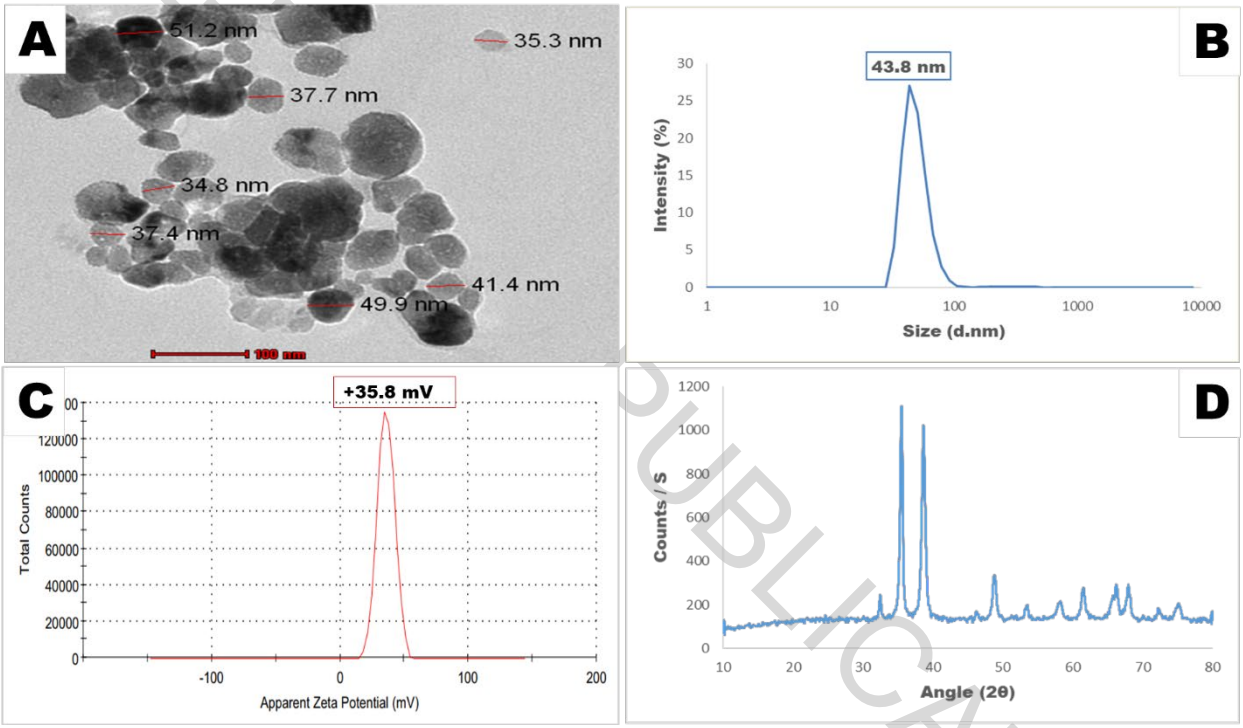

Fig. 3. Characterization of copper-oxide nanoparticles (CuO-NPs). (A) HR-TEM image showing morphology of synthesized CuO-NPs. (B) Particle-size distribution curve illustrating homogeneity of particle dispersion. (C) Zeta-potential analysis indicating positive surface charge and suspension stability. (D) X-ray diffraction (XRD) pattern confirming crystalline CuO phase formation.

3.3. Effect of Chitosan–Silver Nanocomposites (CS–Ag NCs) and Copper Oxide Nanoparticles (CuO–NPs) on Virus Infectivity

As shown in **Fig. 4**, foliar application of CS–Ag NCs and CuO–NPs significantly reduced the incidence of *Hibiscus chlorotic ringspot virus* (HCRSV) infection in *Hibiscus sabdariffa* seedlings compared to infected controls. The generalized linear mixed model (GLMM) indicated significant main effects of both treatment ($\chi^2 = 15.6$, $p = 0.001$) and application timing ($\chi^2 = 7.9$, $p = 0.005$) on infection incidence.

Post-inoculation (curative) treatments exhibited the strongest antiviral effect. At 300 ppm, CS–Ag NCs reduced infection incidence to 70.0 ± 5.0%, while CuO–NPs showed a similar level of reduction (70.0 ± 5.0%). In contrast, pre-inoculation (protective) applications at the same concentration resulted in 58.3 ± 2.9% and 55.0 ± 5.0% infection incidence for CS–Ag NCs and CuO–NPs, respectively, representing the most effective protection within the pre-treatment groups.

Lower concentrations (50–100 ppm) resulted in moderate reductions, with infection incidence ranging from 76.7 ± 2.9% to 70.0 ± 5.0% for CS–Ag NCs and 71.7 ± 2.9% to 65.0 ± 5.0% for CuO–NPs, indicating a dose-dependent inhibitory effect. Statistical analysis revealed that all nanoparticle-treated plants differed significantly from the infected control (100 ± 0.0%), but not significantly from each other within timing categories ($p < 0.05$). According to Tukey's HSD test ($\alpha = 0.05$), treatments sharing the same lowercase letter were not significantly different, whereas treatments with different letters differed significantly, confirming that all nanoparticle treatments significantly reduced infection compared to the infected control, while differences between CS–Ag NCs and CuO–NPs within the same application timing were not statistically significant.

Non-inoculated healthy plants and "healthy + nanoparticle" controls remained symptom-free (0/20 plants) and tested negative for HCRSV by RT-PCR, confirming the absence of cross-contamination. Overall, both nanomaterials demonstrated notable antiviral efficacy. CS–Ag NCs showed numerically lower infection incidence than CuO–NPs in most treatments, particularly under post-inoculation conditions (e.g., 70.0 ± 5.0% vs. 75.0 ± 5.0% at 200 ppm and 70.0 ± 5.0% vs. 70.0 ± 5.0% at 300 ppm), although these differences were not statistically significant according to Tukey's HSD test ($p > 0.05$).

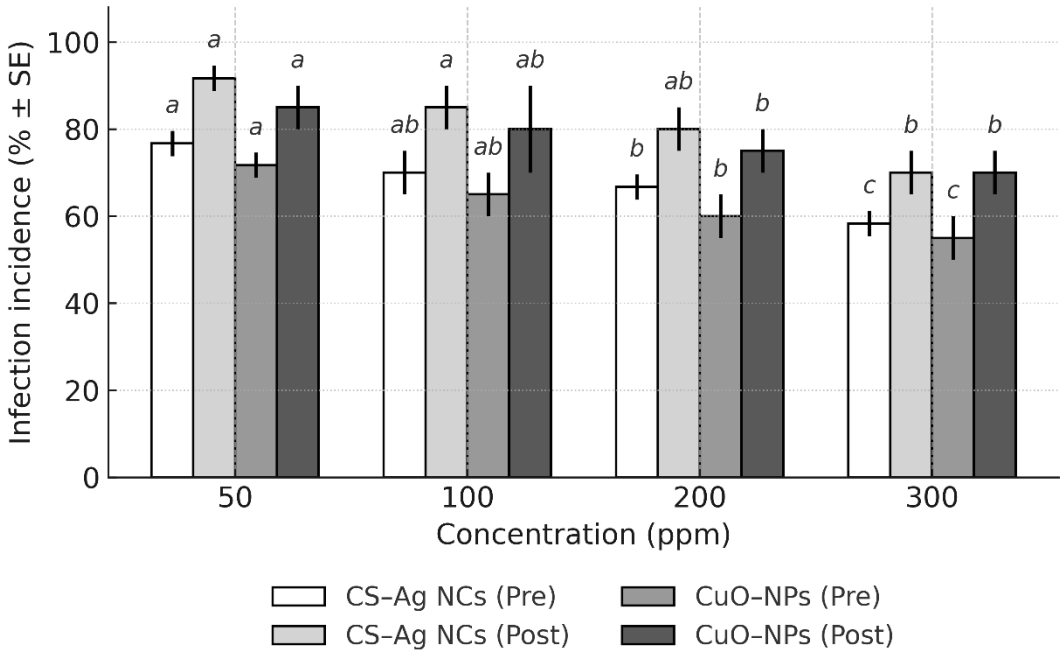

Fig. 4. Effect of chitosan–silver nanocomposites (CS–Ag NCs) and copper oxide nanoparticles (CuO–NPs) on *Hibiscus chlorotic ringspot virus* (HCRSV) infection incidence in *Hibiscus sabdariffa* under greenhouse conditions. Bars represent mean infection percentages (± SE; n = 20 plants, two independent runs of 10 plants each) for four nanoparticle concentrations (50–300 ppm) applied either 24 h before inoculation (Pre; protective) or 24 h after inoculation (Post; curative). White and light-gray bars denote CS-Ag NCs (Pre and Post), whereas medium- and dark-gray bars denote CuO–NPs (Pre and Post). Different lowercase letters above bars indicate statistically significant differences between treatments according to Tukey's HSD test ($\alpha = 0.05$). Both nanomaterials significantly reduced infection in a concentration-dependent manner, with the greatest inhibition observed for CS-Ag NCs at 300 ppm post-inoculation (70 ± 5.0 % infection; ≈ 91.7% inhibition).

3.4. Effect of CS–Ag NCs and CuO–NPs on Bioactive Compounds in Roselle Sepals

As shown in **Fig. 5**, foliar application of CS–Ag NCs and CuO–NPs significantly influenced the biochemical composition of *Hibiscus sabdariffa* sepals compared to the infected control ($p < 0.001$). According to Tukey's HSD test ($\alpha = 0.05$), treatments sharing the same lowercase letter within each biochemical parameter were not significantly different, whereas treatments with different letters differed significantly.

HCRSV infection markedly reduced anthocyanin content to 20.10 ± 1.16 mg g^{-1} DW compared to the healthy control (33.32 ± 1.93 mg g^{-1} DW). Nanoparticle application restored anthocyanin accumulation in infected plants, with CS-Ag NCs and CuO-NPs at 300 ppm reaching 32.11 ± 3.13 and 31.89 ± 2.55 mg g^{-1} DW, respectively. Healthy plants treated with nanoparticles exhibited the highest anthocyanin levels (35.67 ± 1.89 mg g^{-1} DW for CS-Ag NCs and 34.89 ± 3.26 mg g^{-1} DW for CuO-NPs).

Total phenolic content was similarly enhanced by nanoparticle treatments. The highest phenolic concentration was observed in CS-Ag NC–treated plants at 300 ppm (24.74 ± 2.11 mg 100 g^{-1} FW), followed by CuO-NPs at the same concentration (20.68 ± 2.04 mg 100 g^{-1} FW). Both values were significantly higher than those of the infected control (15.68 ± 0.95 mg 100 g^{-1} FW) and the healthy control (14.22 ± 1.30 mg 100 g^{-1} FW).

HCRSV infection significantly increased ascorbic acid content (0.65 ± 0.04 mg 100 g^{-1} FW) relative to the healthy control (0.37 ± 0.03 mg 100 g^{-1} FW), reflecting a stress-induced antioxidant response. Nanoparticle treatments moderated this increase, with ascorbic acid levels at 300 ppm (0.39 ± 0.03 mg 100 g^{-1} FW for CS-Ag NCs and 0.40 ± 0.03 mg 100 g^{-1} FW for CuO-NPs) returning to values statistically comparable to the healthy control.

Titratable acidity increased markedly in infected plants (4.26 ± 0.22%) compared to the healthy control (2.19 ± 0.17%). Both nanoparticles significantly reduced acidity at 300 ppm, yielding 2.17 ± 0.19% for CS-Ag NCs and 2.15 ± 0.16% for CuO-NPs, with no significant difference between nanoparticle types.

Both nanomaterials effectively alleviated virus-induced biochemical disruption in roselle sepals. Although CS-Ag NC-treated plants tended to show numerically higher anthocyanin and phenolic contents than CuO-NP–treated plants at comparable concentrations, these differences were not statistically significant according to Tukey's HSD test ($p > 0.05$).

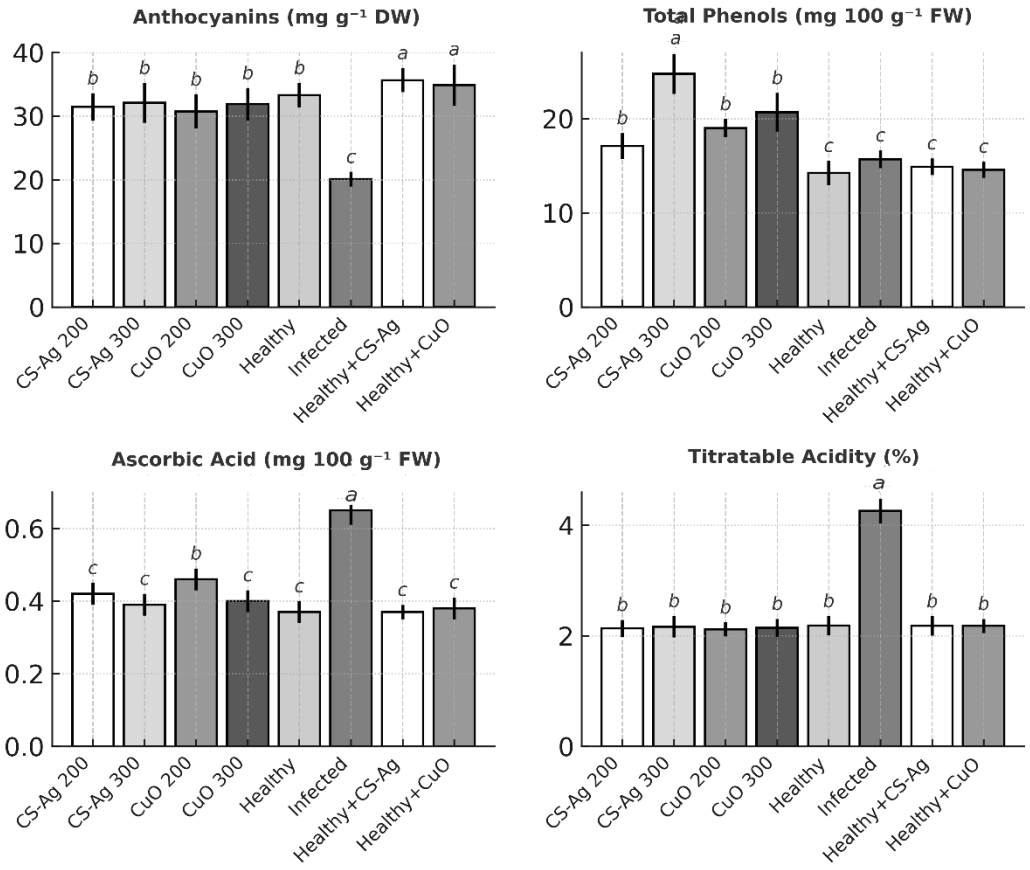

Fig. 5. Effect of chitosan–silver nanocomposites (CS–Ag NCs) and copper oxide nanoparticles (CuO–NPs) on biochemical traits of *Hibiscus sabdariffa* sepals. Bars represent mean values (± SE; n = 3 biological replicates per treatment, each measured in technical triplicate). (A) Anthocyanins (mg g^{-1} DW), (B) total phenols (mg 100 g^{-1} FW), (C) ascorbic acid (mg 100 g^{-1} FW), and (D) titratable acidity (% citric acid equivalents). Different lowercase letters above bars denote statistically significant differences between treatments according to one-way ANOVA followed by Tukey's HSD test ($\alpha = 0.05$). Foliar application of CS-Ag NCs and CuO-NPs significantly restored anthocyanin and phenolic contents while normalizing ascorbic acid and titratable acidity compared to infected controls, indicating effective mitigation of virus-induced oxidative stress and restoration of metabolic homeostasis in roselle sepals.

3.5. Effect of CS-Ag NCs and CuO-NPs on Antioxidant Enzyme Activities

As shown in **Fig. 6**, foliar application of chitosan–silver nanocomposites (CS-Ag NCs) and copper oxide nanoparticles (CuO-NPs) significantly affected antioxidant enzyme activities in *Hibiscus sabdariffa* leaves infected with *Hibiscus chlorotic ringspot virus* (HCRSV) ($p < 0.001$). According to Tukey's HSD test ($\alpha = 0.05$), treatments sharing the same lowercase letter within each enzyme were not significantly different, whereas treatments with different letters differed significantly.

CAT activity was higher in infected plants than in healthy controls. Post-inoculation application of CS-Ag NCs at 300 ppm resulted in the highest CAT activity (7.69 ± 0.77 U mg^{-1} FW), followed by CuO–NPs at the same concentration (6.90 ± 0.69 U mg^{-1} FW). The infected control recorded 6.25 ± 0.62 U mg^{-1} FW. Pre-inoculation treatments produced intermediate CAT activities, ranging from approximately 4.4 to 4.7 U mg^{-1} FW.

POX activity increased markedly following nanoparticle treatments. The highest POX activity was observed in post-inoculated CS-Ag NC–treated plants at 300 ppm (42.55 ± 4.25 U mg^{-1} FW), followed by post-inoculated CuO-NP–treated plants (39.30 ± 3.93 U mg^{-1} FW). In contrast, the infected control exhibited substantially lower POX activity (15.61 ± 1.56 U mg^{-1} FW).

PAL activity was significantly higher in nanoparticle-treated plants than in the infected control. The maximum PAL activity was recorded in post-inoculated CS-Ag NC–treated plants (497.9 ± 49.8 U mg^{-1} FW), while the infected control showed 365.1 ± 36.5 U mg^{-1} FW. Pre-inoculation treatments also resulted in elevated PAL activities, ranging from approximately 460 to 480 U mg^{-1} FW.

Across treatments, CS-Ag NCs showed numerically higher CAT, POX, and PAL activities than CuO-NPs under post-inoculation conditions; however, these differences were not statistically significant according to Tukey's HSD test ($p > 0.05$).

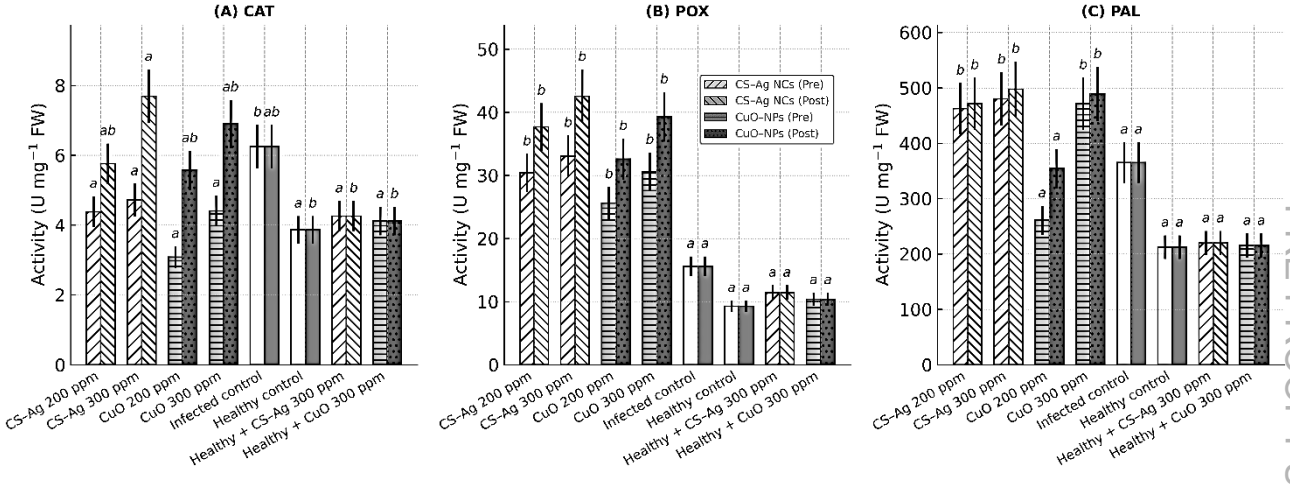

Fig. 6. Effect of chitosan–silver nanocomposites (CS-Ag NCs) and copper oxide nanoparticles (CuO-NPs) on antioxidant enzyme activities in *Hibiscus sabdariffa* leaves infected with *Hibiscus chlorotic ringspot virus* (HCRSV) under pre- and post-inoculation treatments. Bars represent mean enzyme activities (± SE; n = 20 plants from two independent runs). (A) Catalase (CAT), (B) Peroxidase (POX), and (C) Phenylalanine ammonia-lyase (PAL). Each treatment shows paired bars for pre- (lighter shade) and post-inoculation (darker shade) applications. Different lowercase letters above bars indicate significant differences between treatments according to Tukey's HSD test (α = 0.05). Both nanoparticles enhanced antioxidant enzyme activities relative to the infected control, with CS-Ag NCs exhibiting greater induction, particularly in POX and PAL-under post-inoculation conditions, reflecting stronger oxidative-stress detoxification and defense activation in roselle.

3.6 Effect of CS–Ag NCs and CuO–NPs on Roselle Growth and Yield

As shown in **Table 2**, foliar application of CS-Ag NCs and CuO-NPs significantly affected growth and yield parameters of *Hibiscus sabdariffa* plants infected with HCRSV ($p < 0.001$). According to Tukey's HSD test (α = 0.05), values sharing the same superscript letter within each parameter were not significantly different, whereas values with different letters differed significantly.

HCRSV infection reduced sepal fresh weight to 133.2 ± 4.2 g plant^{-1}. Nanoparticle-treated plants showed higher sepal fresh weights, with CS-Ag NCs at 300 ppm recording 222.6 ± 7.1 g plant^{-1} and CuO–NPs at 300 ppm recording 221.4 ± 7.0 g

plant⁻¹. Healthy plants treated with CS–Ag NCs at 300 ppm recorded the highest sepal fresh weight (230.5 ± 7.3 g plant⁻¹).

The infected control exhibited the lowest number of branches (7.4 ± 0.2 branches plant⁻¹). Application of CS–Ag NCs at 200–300 ppm resulted in 11.9–12.1 branches plant⁻¹, while CuO–NPs at 300 ppm produced 11.6 ± 0.3 branches plant⁻¹. The healthy + CS-Ag NCs treatment showed the highest branching value (14.8 ± 0.5 branches plant⁻¹), compared to 12.5 ± 0.4 branches plant⁻¹ in the untreated healthy control.

Plant height was reduced to 160.1 ± 5.1 cm in infected plants. Nanoparticle treatments increased plant height to 199.8 ± 6.3 cm for CS-Ag NCs at 300 ppm and 198.5 ± 6.3 cm for CuO–NPs at the same concentration. Healthy plants treated with CS-Ag NCs reached a height of 205.7 ± 6.5 cm.

Across treatments, CS-Ag NCs showed numerically higher sepal fresh weight, branch number, and plant height than CuO-NPs at comparable concentrations; however, these differences were not statistically significant according to Tukey's HSD test ($p > 0.05$).

Table 2. Effect of CS-Ag NCs and CuO-NPs on Roselle Growth and Yield

Treatment	Conc. (ppm)	Sepal FW (g/plant ± SE)	Branches (no. ± SE)	Plant Height (cm ± SE)
CS–Ag NCs	50	217.4 ± 6.9^{g}	9.1 ± 0.3^{e}	185.3 ± 5.9^{f}
CS–Ag NCs	100	219.5 ± 7.0^{f}	10.3 ± 0.3^{d}	196.4 ± 6.2^{e}
CS–Ag NCs	200	220.8 ± 7.0^{e}	11.9 ± 0.4^{b}	197.6 ± 6.2^{d}
CS–Ag NCs	300	222.6 ± 7.1^{d}	12.1 ± 0.4^{b}	199.8 ± 6.3^{c}
CuO–NPs	50	216.7 ± 6.9^{h}	8.2 ± 0.3^{f}	183.7 ± 5.8^{f}
CuO–NPs	100	219.1 ± 6.9^{f}	9.8 ± 0.3^{e}	194.9 ± 6.2^{e}
CuO–NPs	200	220.3 ± 7.0^{e}	10.9 ± 0.3^{c}	196.3 ± 6.2^{d}
CuO–NPs	300	221.4 ± 7.0^{e}	11.6 ± 0.3^{c}	198.5 ± 6.3^{c}
Healthy control	–	225.4 ± 7.1^{c}	12.5 ± 0.4^{b}	202.3 ± 6.4^{b}
Infected control	–	133.2 ± 4.2^{l}	7.4 ± 0.2^{g}	160.1 ± 5.1^{h}
Healthy + CS–Ag NCs	300	230.5 ± 7.3^{a}	14.8 ± 0.5^{a}	205.7 ± 6.5^{a}
Healthy + CuO–NPs	300	227.3 ± 7.2^{b}	13.5 ± 0.4^{a}	203.5 ± 6.4^{b}

Values represent means ± standard error (SE) of n = 10 plants from two independent runs. Different superscript letters within a column indicate significant differences between treatments according to Tukey's HSD test (α = 0.05) on model estimated marginal means (EMMs). F- and *p*-values correspond to the two-way ANOVA results for treatment effects.

3.7. Nanomaterial Treatments Modulate Host Gene Expression in HCRSV-Infected Plants

Gene expression was quantified by quantitative real-time PCR, and relative transcript levels were calculated using the $2^{-\Delta\Delta Ct}$ method. Fold-change values are presented to illustrate treatment-dependent transcriptional responses of APS kinase (APK), adenylylsulfate reductase (*APR*), and sulfite oxidase (*SO*) in *Hibiscus sabdariffa* following foliar application of chitosan–silver nanocomposites (CS-Ag NCs) and copper oxide nanoparticles (CuO-NPs) at 50–300 ppm, applied either before (protective) or after (curative) inoculation with Hibiscus chlorotic ringspot virus (HCRSV) (**Fig. 7**).

APK expression (**Fig. 7A**) showed clear concentration- and timing-dependent modulation. Transcript levels were modestly elevated in infected plants compared to the healthy control (≈3.5-fold). The strongest induction was observed in 200 ppm post-inoculation CS-Ag NCs (≈7.5-fold), followed by 300 ppm post-inoculation CuO-NPs (≈6.5-fold). Moderate induction occurred at 100 ppm pre-inoculation CuO-NPs (≈4.7-fold), whereas low-dose treatments (50 ppm), particularly under pre-inoculation conditions, resulted in minimal activation or slight repression relative to the healthy control. These patterns indicated that effective APK activation required threshold nanomaterial concentrations, with curative CS-Ag NC application being most effective. APR expression (**Fig. 7B)** displayed a pronounced biphasic response, with maximal induction restricted to intermediate nanoparticle concentrations, consistent with redox-sensitive regulation of reductive sulfur flux rather than sustained immune priming. The highest transcript accumulation was detected in 100 ppm pre-inoculation CS-Ag NCs (≈55.8-fold), representing the strongest response observed among all genes analyzed. Substantial induction was also recorded in 100 ppm post-inoculation CuO-NPs (≈13.5-fold) and in 200 ppm post-inoculation treatments of both nanomaterials (≈7–11-fold). In contrast, APR expression remained low at 50 ppm and declined again at 300 ppm,

suggesting that APR activation was optimal within a narrow concentration range and was sensitive to excessive or insufficient stress.

SO expression (**Fig. 7C**) was consistently upregulated across most nanomaterial treatments relative to the healthy control. The highest induction occurred in 200 ppm post-inoculation CS-Ag NC**s** (≈14.4-fold), followed by 200 ppm pre-inoculation CuO-NPs (≈10.8-fold) and 300 ppm post-inoculation CuO-NPs (≈7.9-fold). Moderate induction was observed at 100 ppm pre-inoculation treatments for both nanomaterials (≈6–7-fold), whereas lower concentrations (50 ppm) resulted in only weak transcript accumulation (≈2–4-fold). These results indicate that *SO* was strongly responsive to nanomaterial-mediated stress, particularly under curative application at intermediate concentrations.

Collectively, these transcriptional profiles demonstrate that CS-Ag NCs and CuO-NPs modulate sulfur-related defense genes in *H. sabdariffa* in a gene-specific, concentration-dependent, and application-timing-dependent manner. Notably, post-inoculation treatments at intermediate concentrations (100–200 ppm) were consistently associated with the strongest activation of *APK*, *APR*, and *SO*, supporting a role for nanomaterial-mediated reinforcement of host defense pathways during active viral infection.

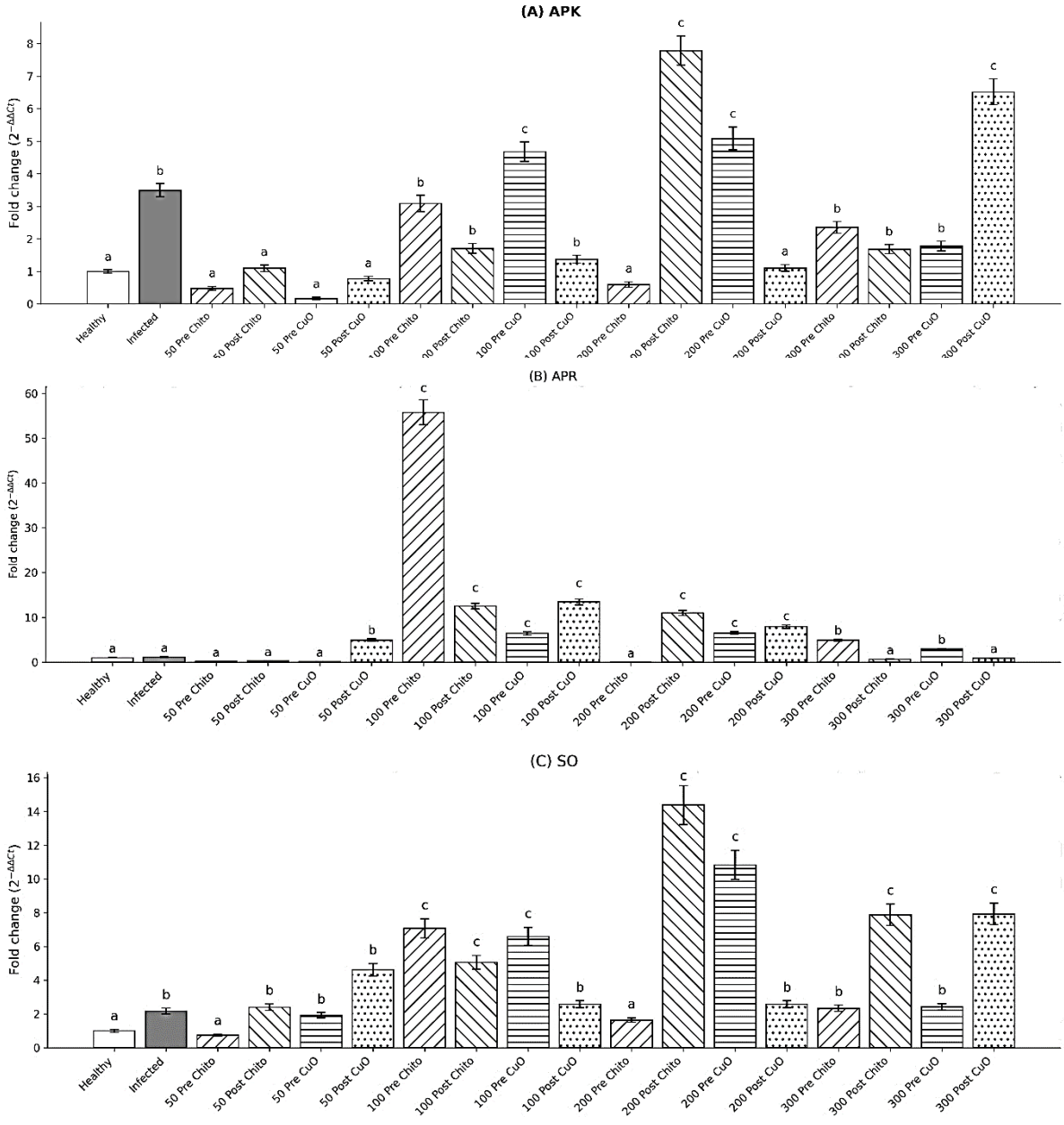

Fig. 7. Relative expression profiles of (A) *APK*, (B) *APR*, and (C) *SO* genes in *Hibiscus sabdariffa* following foliar application of chitosan–silver nanocomposites (CS-Ag NCs) and copper oxide nanoparticles (CuO-NPs) applied either before (Pre; protective) or after (Post; curative) inoculation with *Hibiscus chlorotic ringspot virus* (HCRSV). Gene expression levels are presented as fold change calculated using the $2^{-\Delta\Delta Ct}$ method, normalized to the reference gene actin and expressed relative to the healthy control. Letter annotations (a–c) denote relative expression categories based on fold-change magnitude: a, low or no induction (≤2-fold); b, moderate induction (2–5-fold); c, strong induction (>5-fold). RT-qPCR was conducted as a single analytical run; therefore,

values are presented without error bars and are intended to illustrate comparative expression trends rather than statistical significance.

4. Discussion

Metal-based nanomaterials-especially chitosan-silver composites and copper oxide systems-are increasingly being recognized as dual-mode antivirals in plants, acting both directly on virions and indirectly by priming host immunity via redox and defense signaling. Contemporary reviews describe disruption of viral particle integrity, interference with host–virus recognition and activation of antioxidant/defense enzymes as convergent routes to protection **(Warghane *et al*. 2024; Lu *et al*. 2024)**. In this study, antiviral efficacy was assessed indirectly through infection incidence and symptom expression, while defense priming was evaluated independently through biochemical and transcriptional markers; viral titers were not quantified directly.

Consistent with current frameworks describing nanomaterials as plant immunomodulators rather than solely virucidal agents, the observed efficacy of CS-Ag NCs and CuO-NPs in reducing HCRSV infection under greenhouse conditions can be interpreted as a consequence of optimized dose-timing interactions that favor host defense activation. The superior performance of post-inoculation applications, particularly at higher concentrations, supports the concept that nanomaterials are most effective when applied during early stages of viral replication, where they can amplify endogenous defense responses rather than function exclusively as preventive barriers. Similar post-infection efficacy has been documented for chitosan–silver formulations against *Alfalfa mosaic virus* and *Zucchini yellow mosaic virus*, where curative applications resulted in strong suppression of disease development, reinforcing the role of chitosan-based nanocomposites as defense-priming agents (**El-Ganainy *et al*. 2023; Vasquez-Gutierrez *et al*. 2025**). In parallel, copper-oxide nanoparticles have been shown to exert antiviral activity through both direct and indirect mechanisms, including physical disruption of viral particles and modulation of host redox status, as demonstrated for *Tobacco mosaic virus* at comparable concentrations (**Rajeshkumar *et al*. 2025**). Together, these studies place the present findings within a broader, emerging consensus that metal-based nanomaterials achieve antiviral protection primarily by enhancing host immune competence, with treatment timing and

formulation playing decisive roles in determining efficacy. Considering antiviral efficacy independently of defense markers, both CS-Ag NCs and CuO-NPs reduced HCRSV infection incidence under greenhouse conditions, with post-inoculation applications showing superior performance.

At the biochemical level, the coordinated enhancement of PAL, POX, and CAT activities, together with elevated phenolics and anthocyanins, reflects a shift toward reinforced antioxidant and phenylpropanoid metabolism. This response is now widely recognized as a hallmark of nanomaterial-induced systemic resistance, particularly for chitosan and nano-chitosan systems in solanaceous and malvaceous crops (**Masood *et al.* 2024; Warghane *et al.* 2024**). Rather than restating enzyme increases, the key implication is that CS-Ag NCs appear to stabilize ROS homeostasis, allowing signaling-level oxidative bursts without progressing to cellular damage, a balance essential for effective antiviral defense.

By contrast, the responses elicited by CuO-NPs were strongly shaped by dose and application context, reflecting a narrower therapeutic window than CS-Ag NCs. Rather than inducing uniform defense activation, CuO-NP treatments produced variable transcriptional outcomes, consistent with the dual role of copper-based nanomaterials as both immune stimulants and redox-active stressors. Recent studies indicate that CuO-NPs can enhance antiviral resistance by triggering oxidative and sulfur-associated defense pathways, but excessive or suboptimal dosing may shift cellular metabolism toward stress compensation rather than sustained immune priming. This balance is particularly evident in sulfur assimilation pathways, where differential allocation between reductive (APR-mediated) and regulatory branches has been shown to depend on intracellular redox status. Contemporary nano-immunomodulation frameworks therefore, emphasize that engineered nanomaterials can either potentiate or constrain plant innate immunity depending on dose, timing, and formulation, highlighting the importance of precise application strategies for copper-based systems (**Aseel *et al.* 2024**).

From a plant-performance perspective, a dose-responsive reduction in disease incidence was observed across both nanomaterial treatments under greenhouse conditions, based on symptom expression and infection frequency. As viral titers were

not quantified directly, this reduction reflected indirect antiviral efficacy rather than measured suppression of viral accumulation.

From a defense-priming perspective, nanoparticle treatments were associated with coordinated changes in antioxidant enzyme activities, secondary metabolite accumulation, and sulfur-related gene expression.

The superior curative performance of CS-Ag NCs is consistent with mounting evidence that chitosan-based nanomaterials preferentially activate systemic acquired resistance (SAR)-related pathways, thereby reinforcing plant immunity during active infection. Importantly, the absence of visible phytotoxic symptoms under the applied conditions suggested that effective antiviral priming can be achieved without compromising plant growth. Nevertheless, recent studies emphasize that prolonged or excessive exposure to metal-based nanomaterials, particularly metal oxides, may disrupt membrane integrity, redox balance, and nutrient acquisition, underscoring the need for careful optimization of application dose and timing. Accordingly, environmental risk assessment and exposure-window refinement are essential steps toward translating nano-enabled antiviral strategies into safe and sustainable crop-protection practices (**Mosa and El-Abeid 2023**).

Integrating transcriptional outputs with biochemical and phenotypic responses reveals a clear functional distinction between sulfur-redox regulation and reductive sulfur assimilation under nanomaterial treatment. Sustained induction of *SO* and *APK*, particularly under post-inoculation CS-Ag NC applications, supports reinforcement of sulfur-linked redox buffering and controlled ROS detoxification, processes essential for effective antiviral defense signaling. In contrast, *APR* exhibited a tightly constrained, biphasic response, with strong induction limited to intermediate concentrations and attenuation at both low and high doses. This pattern is consistent with redox-sensitive metabolic reallocation within the sulfur assimilation network rather than uniform immune activation. Such differential regulation aligns with contemporary models of nano-enabled immunomodulation, wherein engineered nanomaterials fine-tune host defense pathways according to intracellular redox context, balancing immune activation against metabolic stress compensation (**Hasanuzzaman *et al.* 2020; Warghane *et al.* 2024**). In particular, sustained activation of sulfur-oxidation and

regulatory nodes suggests stabilization of redox homeostasis during viral challenge, enabling effective deployment of downstream defense such as phenylpropanoid metabolism and ROS detoxification, a mechanism previously linked to chitosan- and nanoparticle-induced immune priming (**Masood *et al*. 2024; El-Ganainy *et al*. 2023**). By contrast, regulation of the reductive sulfur branch displayed a non-linear response to nanomaterial exposure, indicative of redox-sensitive metabolic reallocation rather than uniform immune priming. Such biphasic behavior is widely reported in stress-regulated sulfur assimilation, where moderate oxidative cues enhance reductive flux to support thiol and glutathione pools, whereas excessive or insufficient stimulation constrains pathway activity to prevent metabolic overload (**Hasanuzzaman *et al*. 2020; Masood *et al*. 2024**). This differential regulation of sulfur-metabolic nodes aligns with contemporary nano-immunomodulation models proposing that engineered nanomaterials can either reinforce or constrain plant immunity depending on dose, timing, and intracellular redox context, thereby shaping the balance between defense activation and stress compensation (**Aseel *et al*. 2024; Warghane *et al*. 2024**).

Finally, the roselle-HCRSV pathosystem examined here is consistent with recent molecular and epidemiological characterizations of HCRSV in *Hibiscus* spp., reinforcing its relevance for defining effective dose–response windows and treatment timing in antiviral interventions (**Warghane *et al*. 2024; Shafie 2019**). Framed within this biologically relevant system, the present findings suggest that nano-enabled defense priming can be optimized by aligning nanomaterial formulation and application timing with host immune activation dynamics. Moving beyond proof-of-concept, future research should prioritize quantitative assessment of viral suppression and systems-level mapping of host responses to contextualize sulfur-redox regulators (*SO/APK/APR*) within broader SA/JA/ET signaling networks. Equally important for field translation is understanding the environmental fate and persistence of nanomaterials in soil–plant systems. Comparative evaluation of biogenic or surface-functionalized formulations that preserve immune-priming efficacy while reducing metal ion release and ecological footprint will be critical for advancing nano-enabled plant immunomodulation toward sustainable, field-deployable crop protection strategies (**Aseel *et al*. 2024; Mosa and El-Abeid 2023**).

Across greenhouse evaluations, the absence of visible phytotoxic symptoms under effective antiviral dosing indicates that both CS-Ag NCs and CuO-NPs can be applied within a safety margin that preserves plant performance under controlled conditions. Interpreted mechanistically, this suggests that antiviral efficacy at optimized doses was achieved through immune priming rather than nonspecific oxidative injury. Nonetheless, recent studies caution that metal-based nanomaterials may elicit adverse effects under excessive or prolonged exposure, including membrane lipid peroxidation, disruption of ion homeostasis, and altered nutrient acquisition, particularly for copper- and silver-containing systems (**Mosa and El-Abeid 2023; Aseel *et al.* 2024**). Beyond plant-level responses, environmental considerations are equally critical, as nanoparticle aging processes, such as agglomeration and partial dissolution to Ag^{+} or Cu^{2+}, along with interactions with soil organic matter and the rhizosphere microbiome, can substantially modify persistence and bioavailability. Accordingly, advancing nano-enabled antiviral strategies toward field use will require defining safe exposure windows under season-long applications, monitoring metal accumulation and antioxidant status in plant-soil compartments, and prioritizing greener or surface-functionalized formulations (e.g., biogenic capping or chitosan-coated CuO) that retain immune-priming efficacy while minimizing ionic release and off-target ecological effects (**Warghane *et al.* 2024**).

5. Conclusion

This study demonstrated that chitosan–silver nanocomposites (CS-Ag NCs) and copper oxide nanoparticles (CuO-NPs) provided effective antiviral protection against *Hibiscus chlorotic ringspot virus* in *Hibiscus sabdariffa* through modulation of host defense mechanisms. Both nanomaterials reduced infection incidence and enhanced antioxidant and phenylpropanoid metabolism, while transcriptional profiling revealed sustained activation of sulfur-redox regulators (*SO* and *APK*) under CS-Ag NC treatments and more dose-dependent, stress-responsive transcriptional patterns under CuO-NP exposure. From a plant-protection perspective, the strong curative efficacy and absence of visible phytotoxicity at operational doses highlight CS-Ag NCs as a promising nano-enabled strategy for managing viral diseases in high-value crops. Nevertheless, field validation, direct viral load quantification, and environmental fate assessments remain essential to translate these findings into safe, sustainable, and scalable crop-protection applications.

Conflict of Interest Statement: The authors declare that there are no conflicts of interest.

Funding Statement: No specific grant was received for this study.

Data Availability: All data are available from the corresponding author

Ethics Statement: This study did not involve human or animal participants; hence, ethical approval was not required.

References

Abdelkader H. S., Kheder A. A.A., Amin H. A., Shafie R. M. 2025. A comparative study of the antiviral effects of biogenic silver nanoparticles and nanosilica ($nSiO_2$) against Leek yellow stripe virus on *Allium sativum* L. European Journal of Plant Pathology 171(3): 509-530. DOI: https://doi.org/10.1007/s10658-024-02965-3

Abdelkhalek A., Qari S. H., Abu-Saied M. A. A.-R., Khalil A. M., Younes H. A., Nehela Y., Behiry S. I. 2021. Chitosan nanoparticles inactivate Alfalfa mosaic virus replication and boost innate immunity in *Nicotiana glutinosa* plants. Plants 10(12): 2701. DOI: https://doi.org/10.3390/plants10122701

Abou-Sreea A., Roby M. H., Abdelkader H. A., Mahdy H. A., Abdou N. M., El-Tahan A. M., El-Saadony M. T., El-Tarabily H. A., El-Saadony F. M. 2022. Improvement of selected morphological, physiological and biochemical parameters of roselle (*Hibiscus sabdariffa* L.) grown under different salinity levels using potassium silicate and *Aloe saponaria* extract. The Plant Journal 11(4): 1–20. DOI: https://doi.org/10.3390/plants11040497

Ali B. H., Wabel N. A. I., Blunden G. 2005. Phytochemical, pharmacological and toxicological aspects of *Hibiscus sabdariffa* L.: A review. Phytotherapy Research 19(5): 369–375. DOI: https://doi.org/10.1002/ptr.1628

Anand T., Chandrasekaran A., Kuttalam S., Raghuchander T., Prakasam V., Samiyappan R. 2007. Association of some plant defense enzyme activities with systemic resistance to early blight and leaf spot induced in tomato plants by azoxystrobin and Pseudomonas fluorescens. Journal of Plant Interactions 2(4): 233–244. DOI: https://doi.org/10.1080/17429140701799954

Anusuya S., Banu K. N. 2016. Silver–chitosan nanoparticles induced biochemical variations of chickpea (*Cicer arietinum* L.). Biocatalysis and Agricultural Biotechnology 8: 39–44. DOI: https://doi.org/10.1016/j.bcab.2016.08.005

Aseel D., Rabie M., El-Far A., Abdelkhalek A. 2024. Antiviral properties and molecular docking studies of eco-friendly biosynthesized copper oxide nanoparticles against Alfalfa mosaic virus. BMC Plant Biology 24(1): 1089. DOI: https://doi.org/10.1186/s12870-024-05802-1

Association of Official Agricultural Chemists (A.O.A.C.) 1965. Official Methods of Analysis. 10th ed. Association of Official Agricultural Chemists, Washington, D.C., USA.

Babajide J. M., Bodunde J. G., Salami A. A. 2004. Quality and sensory evaluation of processed calyces of six varieties of roselle (*Hibiscus sabdariffa* L.). Nigerian Journal of Horticultural Science 9: 110–115. DOI: https://doi.org/10.4314/njhs.v9i1.3388

Babu B., Nair R. S., Angelo J. M., Mathai V., Vineet R. V. 2017. Evaluation of the efficacy of chitosan-silver nanocomposite on *Candida albicans* when compared to three different antifungal agents in combination with standard irrigation protocol: An ex vivo study. Saudi Endodontic Journal 7(2): 87–91. DOI: https://doi.org/10.4103/1658-5984.202949

Bhandari G., Dhasmana A., Chaudhary P., Gupta S., Gangola S., Gupta A., Rustagi S., Shende S. S., Rajput V. D., Minkina T., Malik S. 2023. A perspective review on green nanotechnology in agro ecosystems: Opportunities for sustainable agricultural practices and environmental remediation. Agriculture 13(5): 668. DOI: https://doi.org/10.3390/agriculture13050668

Brunt A., Spence N. J. 2000. The natural occurrence of *Hibiscus chlorotic ringspot virus* (Carmovirus; Tombusviridae) in aibika or bele (*Abelmoschus manihot*) in some South Pacific Island countries. New Disease Reports 11: 20. DOI: https://doi.org/10.1046/j.1365-3059.2000.00501.x

Cai L., Liu C., Fan G., Liu C., Sun X. 2019. Preventing viral disease by zinc oxide nanoparticles through directly deactivating Tobacco mosaic virus and activating plant immunity in *Nicotiana benthamiana*. Environmental Science: Nano 6(12): 3653–3669. DOI: https://doi.org/10.1039/C9EN00850K

Chandra S., Chakraborty N., Dasgupta A., Sarkar J., Panda K., Acharya K. 2015. Chitosan nanoparticles: A positive modulator of innate immune responses in plants. Scientific Reports 5: 15195. DOI: https://doi.org/10.1038/srep15195

Chen Z., Meng H., Xing G., Chen C., Zhao Y., Jia G., Wan L. 2006. Acute toxicological effects of copper nanoparticles in vivo. Toxicology Letters 163(2): 109–120. DOI: https://doi.org/10.1016/j.toxlet.2005.10.003

Davydova V. N., Nagorskaya V. P., Gorbach V. I., Kalitnik A. A., Reunov A. V., Solov'eva T. F., Ermak I. M. 2011. Chitosan antiviral activity: Dependence on structure and depolymerization method. Applied Biochemistry and Microbiology 47(2): 103–108. DOI: https://doi.org/10.1134/S0003683811020036

Derbalah A., Abdelsalam I., Behiry S. I., Abdelkhalek A., Abdelfatah M., Ismail S., Elsharkawy M. M. 2022. Copper oxide nanostructures as a potential method for control of zucchini yellow mosaic virus in squash. Pest Management Science 78(8): 3585–3595. DOI: https://doi.org/10.1002/ps.6991

Devi P. R., Doraiswamy S., Nakkeeran S., Rabindran R., Ganapathy T., Ramiah M. 2004. Antiviral action of *Harpulia cupanioides* and *Mirabilis jalapa* against Tomato spotted wilt virus in tomato. Archives of Phytopathology and Plant Protection 37(4): 245–259. DOI: https://doi.org/10.1080/03235400410001714939

Du C. T., Francis F. J. 1973. Anthocyanin of roselle. Journal of Food Science 38: 810–812.

Dutta P., Kumari A., Mahanta M., Biswas K. K., Dudkiewicz A., Thakuria D., Abdelrhim A. S., Singh S. B., Muthukrishnan G., Sabarinathan K. G., Mandal M. K., Mazumdar N. 2022. Advances in nanotechnology as a potential alternative for plant viral disease management. Frontiers in Microbiology 13: 935193. DOI: https://doi.org/10.3389/fmicb.2022.935193

El Gamal A. Y., Tohamy M. R., Abou-Zaid M. I., Atia M. M., El Sayed T., Farroh K. Y. 2022. Silver nanoparticles as a viricidal agent to inhibit plant-infecting viruses and disrupt their acquisition and transmission by aphid vectors. Archives of Virology 165(1): 85–97. DOI: https://doi.org/10.1007/s00705-019-04483-8

El-Ganainy S. M., Soliman A. M., Ismail A. M., Sattar M. N., Farroh K. Y., Shafie R. M. 2023. Antiviral activity of chitosan nanoparticles and chitosan silver nanocomposites against Alfalfa mosaic virus. Polymers 15(13): 2961. DOI: https://doi.org/10.3390/polym15132961

Elsahhar S., Shahba M., Elsayed T., Mikhail M., Galal A. 2022. Effect of chitosan nanoparticles on in vitro regeneration and production of Potato virus Y-free plants of potato. Agronomy 12(11): 2901. DOI: DOI: https://doi.org/10.3390/agronomy12112901

El-Shazly M. A., Kobeasy M. I., Altalhi S. H. 2016. Biological, serological and inhibition activity of Tomato spotted wilt virus isolated from tomato plants in the Taif region, Saudi Arabia. Journal of Virological Sciences 13(1): 52–73.

Fasoyiro S. B., Ashaye O. A., Adeola A., Samuel F. O. 2005. Chemical and storability of fruit-flavoured *Hibiscus sabdariffa* drinks. World Journal of Agricultural Sciences 1(2): 165–168.

Fernando S. S. N., Gunasekara C., Holton J. 2018. Antimicrobial nanoparticles: Applications and mechanisms of action. Sri Lankan Journal of Infectious Diseases 8(1): 2–11. DOI: https://doi.org/10.4038/sljid.v8i1.8167

Fuleki T., Francis F. J. 1968. Quantitative methods for anthocyanins. Journal of Food Science 33(1): 78–83. https://doi.org/10.1111/j.1365-2621.1968.tb00887.x

Galdiero S., Falanga A., Vitiello M., Cantisani M., Marra V., Galdiero M. 2011. Silver nanoparticles as potential antiviral agents. Molecules 16(10): 8894–8918. DOI: https://doi.org/10.3390/molecules16108894

Galeazzi M. A., Sgarbieri V. C., Garbieri S., Constantinides M. 1981. Isolation, purification and physicochemical characterization of polyphenol oxidase from banana. Journal of Food Science 46(1): 150–155. DOI: https://doi.org/10.1111/j.1365-2621.1981.tb14556.x

Gao R., Ng F. K. L., Liu P., Wong S. M. 2012. Hibiscus chlorotic ringspot virus coat protein upregulates sulfur metabolism genes for enhanced pathogen defense. Molecular Plant–Microbe Interactions 25(12): 1574–1583. DOI: https://doi.org/10.1094/MPMI-08-12-0203-R

Giannopolitis C. N., Ries S. K. (1977). Superoxide dismutase: Purification and quantitative relationship with water-soluble protein in seedlings. Plant Physiology 59(2): 315–318. DOI: https://doi.org/10.1104/pp.59.2.315

Hassan F. 2009. Response of *Hibiscus sabdariffa* L. to biofertilization treatments. Annals of Agricultural Science (Ain Shams University) 54(2): 437–446.

Hassan O., Chang T. 2017. Chitosan for eco-friendly control of plant disease. Asian Journal of Plant Pathology 11(2): 53–70. DOI: https://doi.org/10.3923/ajppaj.2017.53.70

He X., Xing R., Liu S., Qin Y., Li K., Yu H., Li P. 2021. Improved antiviral activities of amino-modified chitosan derivatives against Newcastle disease virus. Drug and Chemical Toxicology 44(4): 335–340. DOI: https://doi.org/10.1080/01480545.2019.1690475

Kopriva S., Rahimzadeh Karvansara P., Takahashi H. 2024. Adaptive modifications in plant sulfur metabolism over evolutionary time. Journal of Experimental Botany 75(16): 4697–4711. DOI: https://doi.org/10.1093/jxb/erae252

Liu S., Tian W., Liu Z., Wei X., Yuan K., Du W., Cai L. 2024. Biosynthesis of cupric oxide nanoparticles and their antiviral activities against Tobacco mosaic virus by direct virion destruction and induction of plant resistance. Phytopathology Research 6(1): 30. DOI: https://doi.org/10.1186/s42483-024-00250-z

Loeffler H. J., Ponting J. D. 1942. Ascorbic acid. Industrial and Engineering Chemistry, Analytical Edition 14(11): 846–849. https://doi.org/10.1021/i560111a017

López-Velázquez J. C., García-Morales S., López-Sánchez G. P., Montero-Cortés M. I., Uc-Várguez A., Qui-Zapata J. A. 2023. High-density chitosan induces biochemical and molecular responses in *Coffea arabica* during infection with *Hemileia vastatrix*. International Journal of Molecular Sciences 24(22): 16165. DOI: https://doi.org/10.3390/ijms242216165

Lu J. M., Wang X., Muller C. M., Wang H., Lin P. H., Yu Q., Chen C. 2009. Current advances in research and clinical applications of PLGA-based nanotechnology. Expert Review of Molecular Diagnostics 9(4): 325–341. DOI: https://doi.org/10.1586/erm.09.15

Lu Q., Ding Y., Liu W., Liu S. 2025. Viral infections and the glutathione peroxidase family: Mechanisms of disease development. Antioxidants and Redox Signaling 42(10–12): 623–639. DOI: https://doi.org/10.1089/ars.2024.0645

Luna I. Z., Hilary L. N., Chowdhury A. S., Gafur M. A., Khan N., Khan R. A. 2015. Preparation and characterization of copper oxide nanoparticles synthesized by chemical precipitation. Open Access Library Journal 2(3): 1–8.

Maini A., Shah M. A. 2021. Physical properties of nanosized cobalt-doped copper oxide for electronic device applications. International Journal of Ceramic Engineering and Science 3(3): 192–199. DOI: https://doi.org/10.1002/ces2.10100

Malik C. P., Singh M. B. 1980. *Estimation of Total Phenols in Plant Enzymology and Histoenzymology*. Kalyani Publishers, New Delhi, India.

Masood H. A., Qi Y., Zahid M. K., Li Z., Ahmad S., Lv J. M., Shahid M. S., Ali H. E., Ondrasek G., Qi X. 2024. Nano-enabled immunomodulation for enhancing plant resilience against phytopathogens. Frontiers in Plant Science 15: 1445786. DOI: https://doi.org/10.3389/fpls.2024.1445786

Maxwell D. P., Bateman D. F. 1967. Changes in oxidase activities in *Rhizoctonia*-infected bean hypocotyls during lesion development. Phytopathology 57: 132–136.

Mosa M. A., El-Abeid S. E. 2023. Chitosan-loaded copper oxide nanoparticles as antifungal nanocomposites against Fusarium wilt of tomato. Sustainability 15(19): 14295. DOI: https://doi.org/10.3390/su151914295

Nikolova M. P., Chavali M. S. 2020. Metal oxide nanoparticles as biomedical materials. Biomimetics 5(4): 27. DOI: https://doi.org/10.3390/biomimetics5040027

Niu S., Gil-Salas F. M., Tewary S. K., Samales A. K., Johnson J., Swaminathan K., Wong S. 2014. Hibiscus chlorotic ringspot virus coat protein is essential for viral movement but not RNA replication. PLOS ONE 9(11): e113808. DOI: https://doi.org/10.1371/journal.pone.0113808

Przemieniecki S. W., Damszel M., Kosewska O. 2025. Impact of TiO_2 nanoparticles on wheat rhizosphere microbiome structure and function. International Journal of Molecular Sciences 26(2): 685. DOI: https://doi.org/10.3390/ijms26020685

Rajeshkumar R., Moorthy P. S., Raveendran M., Karthikeyan G., Gomathi V., Djanaguiraman M., Abinaya K. 2025. Mitigating plant viruses through nanoparticles: Mechanisms, applications and future perspectives. Plant Nano Biology 100155. DOI: https://doi.org/10.1016/j.plana.2025.100155

Raza M. A. S., Amin J., Valipour M., Iqbal R., Aslam M. U., Zulfiqar B., Elsalahy H. H. 2024. Copper nanoparticles enhance growth and yield of drought-stressed wheat. Scientific Reports 14(1): 14254. DOI: https://doi.org/10.1038/s41598-024-62680-1

Ross I. A. 2003. *Medicinal Plants of the World: Chemical Constituents, Traditional and Modern Medicinal Uses*. Vol. 1. Humana Press, Totowa, New Jersey, USA.

Saito K. 2004. Sulfur assimilatory metabolism: The long and smelling road. Plant Physiology 136(1): 2443–2450. DOI: https://doi.org/10.1104/pp.104.046755

Shafie R. M. 2019. Hibiscus chlorotic ringspot virus affecting roselle in Egypt. Middle East Journal of Applied Sciences 9: 50–62.

Vasquez-Gutierrez U., Frias-Treviño G. A., Aguirre-Uribe L. A., Ramírez-Barrón S. N., Mendez-Lozano J., Hernández-Juárez A., García-Ruíz H. 2025. Nanoparticles and nanocarriers for managing plant viral diseases. Plants 14(20): 3118. DOI: https://doi.org/10.3390/plants14203118

Warghane A., Saini R., Shri M., Andankar I., Ghosh D. K., Chopade B. A. 2024. Application of nanoparticles for management of plant viral pathogens: Current status and future prospects. Virology 592: 109998. DOI: https://doi.org/10.1016/j.virol.2023.109998